Global Journal of researches in engineering
Mechanical and mechanics engineering
Volume 11 Issue 7 Version 1.0 December 2011
Type: Double Blind Peer Reviewed International Research Journal
Publisher: Global Journals Inc. (USA)
Online ISSN: 2249-4596 Print ISSN:0975-5861

Predictive Model of Orthotropic Un-Symmetric Box Cam Based On Deflection And countered by Segments of Circular-Arc Contact Profiles

By Dr. Fathi Al-Shamma, Dr. Louay S. Yousuf
College of Engineering Mech. Eng. Dept.

Abstract - In this paper the principal objective is to find the deflection of orthotropic box cam profile countered by segments of circular-arc due to the effect of contact loading which produce the generate force that induces high contact stress on the cam-surface especially in high-speed machine. In high-speed it can be used the composite cam, since it affects the whole machine performance to improve the wear resistance. Several researchers investigated the effects of cam profile in accuracy and system flexibility on the output motion experimentally; but there is a lake in the theoretical part. The theoretical part has been done with the solution of orthotropic circular plate equation using the harmonic deflection motion of the follower. The cam used in this paper can be seen in composite shifter cam for a motorcycle transmission, composite hollow cam-shafts, the running valve lift with roller followers of a composite cam-shaft, and heavy duty of marine engine. The aim of the present paper is to find the maximum deflection of orthotropic box cam on the boundaries of the three circular-arc contact profiles for flanks and noses of contact follower loadings. The results were arrangement into theoretical part and finite element using software ANSYS 12.1.

Keywords : Orthotropic Cam, Contact Loading, Circular Plate Equation, ANSYS Software, Un-Symmetric Pressure Angles, Box Cam.

GJRE-A Classification :

PREDICTIVE MODEL OF ORTHOTROPIC UN-SYMMETRIC BOX CAM BASED ON DEFLECTION AND COUNTERED BY SEGMENTS OF CIRCULAR-ARC CONTACT PROFILES

Strictly as per the compliance and regulations of:

Predictive Model of Orthotropic Un-Symmetric Box Cam Based On Deflection And countered by Segments of Circular-Arc Contact Profiles

Dr. Fathi Al-Shamma[α], Dr. Louay S. Yousuf [Ω]

Abstract - In this paper the principal objective is to find the deflection of orthotropic box cam profile countered by segments of circular-arc due to the effect of contact loading which produce the generate force that induces high contact stress on the cam-surface especially in high-speed machine. In high-speed it can be used the composite cam, since it affects the whole machine performance to improve the wear resistance. Several researchers investigated the effects of cam profile in accuracy and system flexibility on the output motion experimentally; but there is a lake in the theoretical part. The theoretical part has been done with the solution of orthotropic circular plate equation using the harmonic deflection motion of the follower. The cam used in this paper can be seen in composite shifter cam for a motorcycle transmission, composite hollow cam-shafts, the running valve lift with roller followers of a composite cam-shaft, and heavy duty of marine engine. The aim of the present paper is to find the maximum deflection of orthotropic box cam on the boundaries of the three circular-arc contact profiles for flanks and noses of contact follower loadings. The results were arrangement into theoretical part and finite element using software ANSYS 12.1.

Keywords : Orthotropic Cam, Contact Loading, Circular Plate Equation, ANSYS Software, Un-Symmetric Pressure Angles, Box Cam.

NOMENCLATURES

Normal Letters		
Symbol	Definition	Unit
a_1	Major distance of ellipse axis	m
b_1	Minor distance of ellipse axis	m
a_2	Difference radius of curvatures between ellipse and semi-circle centers	m
C	Particular solution constant	-----------
D_r, D_θ, and $D_{r\theta}$	Radial, tangential, and twisting flexural rigidity	N. m
L	Length of simply-supported beam	M
L_1	Difference length between two points of contact	M
m_1	Single trigonometric of Furrier series	------------
M_r, M_θ, and $M_{r\theta}$	Circular plate bending and twisting moment	N.m
P_o	Maximum contact pressure	$\frac{N}{m^2}$
r, andθ	Polar coordinates	m, Degree
r_1	Radius of clamped cam center	M
q	Loading contact per unit length	$\frac{N}{m}$
W	Circular plate deflection	M
x, y	Cartesian coordinates	M

Greek Letters		
Symbol	Definition	Unit
σ_y	Yield Stress	$\frac{N}{m^2}$
π	Constant (3.1416)	---------
θ_1, θ_2	Angles of the beginning and the ending for both flanks and noses	Degree

Author [α] : Asst. Prof, College of Engineering Mech. Eng. Dept. E-mail : fathi_alshamma@yahoo.com
Author [Ω] : Lect., College of Engineering Mech. Eng. Dept. E-mail : louaysabah79@yahoo.com

I. INTRODUCTION

A new type of composite cam-shafts that obtain an optimum condition valve lift running with roller followers based on it a new composite function cam profile emphatically is developed, in most cases the lobe profile needs to have a concave form (negative radii in the area of the cam lift profile) to improve fullness coefficient, positive and negative peak acceleration and cam-follower contact stress in cam tip; but at the same time the conventional grinding equipment is to suitable to manufacture this type of cam profile, [1, 2].Moreover the mechanical and microstructure properties of cam-shafts surfaces like Brinell, Rockwell, and Vickers hardness tests of Ti Al N/Al N composite film deposited on the profile surface of cam (made of chilled cast iron 45 steel) experimentally and numerically relating with the Ion Beam sputtering deposition, the solidification, and cooling rate technologies, in which the operation temperature can be controlled below the limitation of phases exchanging or at room temperature to avoid phase exchanging deformation and examined the rapid and slow cooling surfaces, rosette like graphite in pearlitic and low ferrite phase on cam hardness to improve the shape and dimension accuracy, [3, 4].In the other hand the cam material (ferrous P/M materials) of a composite shifter hollow cam-shafts for a sequential transmission includes portions formed of a wear resistant material and portions formed of a light weight material using laser surface quenching and discussed the static joining strength and fatigue strength of cam-shafts with different space between tooth. The destroying torsion of the shifter composite cam structure was (20-30) times as many as its actual work torsion, and its fatigue strength to allow the heavier, wear resistant material durable shifter cam, [5, 6]. It can be studied a composite fabricated cam of Al-Sic using cold isostatic compaction and subsequent sintering die casting with a mixture of four different compositions (10, 20, 25, 30)% of Sic powder mixed with Al powders to obtain a high strength to weight ratio and low coefficient of thermal expansion and measured a cam properties like compressive strength, hardness, density and surface roughness, [7]. The fatigue life and microscopic edge cracks is measured for two open-celled foamed polymers having different densities in compression impact using a cam-driven compound pendulum system and observed that the material measurements at constant incident energy included the static compression modulus and peak dynamic stress, which progressively degraded as the number of impacts approached one million, [8].

II. BOX CAM SHAPE

1. *Plate cam or disk cam*:
   The follower moves in a plane perpendicular to the axis of rotation of the camshaft. A translating or a swing arm follower must be constrained to maintain contact with the cam profile.
2. *Grooved cam or closed cam shown in Fig.(1):*
   This is a plate cam with the follower riding in a groove in the face of the cam.

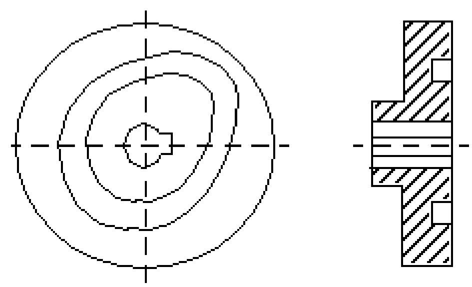

Fig. (1) : Grooved cam.

III. ANALYTICAL PROCEDURE

The general circular plate equation as a function of (r, andθ) coordinates is:

$$\left(\frac{\partial^2}{\partial r^2}+\frac{2}{r}\frac{\partial}{\partial r}\right)*M_r+\left(-\frac{1}{r}\frac{\partial}{\partial r}+\frac{1}{r^2}\frac{\partial^2}{\partial \theta^2}\right)*M_\theta+\left(-\frac{2}{r}\frac{\partial^2}{\partial r\,\partial \theta}-\frac{2}{r^2}\frac{\partial}{\partial \theta}\right)*M_{r\theta}+q=0 \tag{1}$$

Where:

For orthotropic plate, the bending and twist moments are:

$$M_r=-\left[\,D_r*\frac{\partial^2 w}{\partial r^2}+\,D_1*\left(\frac{1}{r}\frac{\partial w}{\partial r}+\frac{1}{r^2}\frac{\partial^2 w}{\partial \theta^2}\right)\right]$$

$$M_\theta=-\left[D_\theta\left(\frac{1}{r}\frac{\partial w}{\partial r}+\frac{1}{r^2}\frac{\partial^2 w}{\partial \theta^2}\right)+D_1*\frac{\partial^2 w}{\partial r^2}\right] \tag{2}$$

$$M_{r\theta}=2*\left[\frac{1}{r}\frac{\partial^2 w}{\partial r\,\partial \theta}-\frac{1}{r^2}\frac{\partial w}{\partial \theta}\right]*D_{r\theta}$$

And;

$$D_r = \frac{E_r * t^3}{12*(\nu_{r\theta} * \nu_{\theta r})}$$

$$D_\theta = \frac{E_\theta * t^3}{12*(\nu_{r\theta} * \nu_{\theta r})}$$

$$D_1 = \frac{\nu_{r\theta} * E_\theta * t^3}{12*(\nu_{r\theta} * \nu_{\theta r})} = \frac{\nu_{\theta r} * E_r * t^3}{12*(\nu_{r\theta} * \nu_{\theta r})}$$

$$D_{r\theta} = \frac{\sqrt{D_r * D_\theta} * (1 - \sqrt{\nu_{r\theta} * \nu_{\theta r}})}{2}$$

The value of first term of eq. (1) is:

$$\left(\frac{\partial^2}{\partial r^2} + \frac{2}{r}\frac{\partial}{\partial r}\right) * M_r = -(D_r * \frac{\partial^4 w}{\partial r^4} + \frac{D_1}{r}\frac{\partial^3 w}{\partial r^3} + \frac{D_1}{r^2}\frac{\partial^4 w}{\partial r^2\,\partial\theta^2} - \frac{2*D_1}{r^3}\frac{\partial^3 w}{\partial r\,\partial\theta^2} + \frac{2*D_1}{r^4}\frac{\partial^2 w}{\partial\theta^2} + \frac{2*D_r}{r}\frac{\partial^3 w}{\partial r^3})$$

And the value of second term of eq. (1) is:

$$\left(-\frac{1}{r}\frac{\partial}{\partial r} + \frac{1}{r^2}\frac{\partial^2}{\partial\theta^2}\right) * M_\theta = -(-\frac{D_\theta}{r^2}\frac{\partial^2 w}{\partial r^2} + \frac{D_\theta}{r^3}\frac{\partial w}{\partial r} + \frac{2*D_\theta}{r^4}\frac{\partial^2 w}{\partial\theta^2} - \frac{D_1}{r}\frac{\partial^3 w}{\partial r^3} + \frac{D_\theta}{r^4}\frac{\partial^4 w}{\partial\theta^4} + \frac{D_1}{r^2}\frac{\partial^4 w}{\partial r^2\,\partial\theta^2})$$

Also the value of third term of eq. (1) is:

$$\left(-\frac{2}{r}\frac{\partial^2}{\partial r\,\partial\theta} - \frac{2}{r^2}\frac{\partial}{\partial\theta}\right) * M_{r\theta} = 2 * D_{r\theta}(-\frac{2}{r^2}\frac{\partial^4 w}{\partial r^2\,\partial\theta^2} + \frac{2}{r^3}\frac{\partial^3 w}{\partial r\,\partial\theta^2} - \frac{2}{r^4}\frac{\partial^2 w}{\partial\theta^2})$$

It can be put the three terms derived above in eq. (1) to obtain:

$$D_r * \frac{\partial^4 w}{\partial r^4} + \frac{2*D_r}{r}\frac{\partial^3 w}{\partial r^3} - \frac{D_\theta}{r^2}\frac{\partial^2 w}{\partial r^2} + \frac{D_\theta}{r^3}\frac{\partial w}{\partial r} + \frac{2*(D_1+2*D_{r\theta})}{r^2}\frac{\partial^4 w}{\partial r^2\,\partial\theta^2} - \frac{2*(D_1+2*D_{r\theta})}{r^3}\frac{\partial^3 w}{\partial r\,\partial\theta^2} + \frac{2*(D_1+D_\theta+2*D_{r\theta})}{r^4}\frac{\partial^2 w}{\partial\theta^2} + \frac{D_\theta}{r^4}\frac{\partial^4 w}{\partial\theta^4} = q \tag{3}$$

The homogenous solution of eq. (1) is as follows:

$$w(r,\theta)_H = A * \sin(r*\theta) + B * \cos(r*\theta) \tag{4}$$

Where:

A and B are constants.

It can be derived the homogenous solution (1, 2, 3, 4) times with respect to r and θ to obtain:

$$\frac{\partial w}{\partial r} = A * \theta * \cos(r*\theta) - B * \theta * \sin(r*\theta)$$

$$\frac{\partial^2 w}{\partial r^2} = -A * \theta^2 * \sin(r*\theta) - B * \theta^2 * \cos(r*\theta)$$

$$\frac{\partial^3 w}{\partial r^3} = -A * \theta^3 * \cos(r*\theta) + B * \theta^3 * \sin(r*\theta)$$

$$\frac{\partial^4 w}{\partial r^4} = A * \theta^4 * \sin(r*\theta) + B * \theta^4 * \cos(r*\theta)$$

$$\frac{\partial^4 w}{\partial r^2\,\partial\theta^2} = -A*\left(-\theta^2*r^2*\sin(r*\theta)+4*\theta*r*\cos(r*\theta)+2*\sin(r*\theta)\right)-B*(-\theta^2*r^2*\cos(r*\theta)-4*\theta*r*\sin(r*\theta)+2*\cos(r*\theta))$$

$$\frac{\partial^3 w}{\partial r\,\partial\theta^2} = A*(-\theta*r^2*\cos(r*\theta)-2*r*\sin(r*\theta))-B*(-\theta*r^2*\sin(r*\theta)+2*r*\cos(r*\theta))$$

$$\frac{\partial^2 w}{\partial\theta^2} = -A*r^2*\sin(r*\theta)-B*r^2*\cos(r*\theta)$$

$$\frac{\partial^4 w}{\partial\theta^4} = A*r^4*\sin(r*\theta)+B*r^4*\cos(r*\theta)$$

After putting the above derivatives in eq. (1) and after simplification to obtain:

$$w(r,\theta)_H = \frac{(2*D_r*\theta^3*r^2+6*D_1*r^2*\theta+12*D_{r\theta}*r^2*\theta-D_\theta*\theta)}{(D_r*\theta^4*r^3+D_\theta*\theta^2*r+2*D_1*r^3*\theta^2+4*D_{r\theta}*r^3*\theta^2-2*D_1*r-2*D_\theta*r-4*D_{r\theta}*r+r^3)}*A*\cos(r*\theta)-\frac{(2*D_r*\theta^3*r^2+6*D_1*r^2*\theta+12*D_{r\theta}*r^2*\theta-D_\theta*\theta)}{(D_r*\theta^4*r^3+D_\theta*\theta^2*r+2*D_1*r^3*\theta^2+4*D_{r\theta}*r^3*\theta^2-2*D_1*r-2*D_\theta*r-4*D_{r\theta}*r+r^3)}*B*\sin(r*\theta) \quad (5)$$

And the particular solution is:

$$w(r,\theta)_P = C*r*\theta \quad (6)$$

Put eq. (6) in plate equation eq. (1) and find the value of constant (C):

$$C = \frac{q*r^3}{\theta*D_\theta}$$

$$w(r,\theta)_P = \frac{q*r^4}{D_\theta} \quad (7)$$

The complementary solution of deflection is as below:

$$w(r,\theta) = w(r,\theta)_H + w(r,\theta)_P$$

$$w(r,\theta) = \frac{(2*D_r*\theta^3*r^2+6*D_1*r^2*\theta+12*D_{r\theta}*r^2*\theta-D_\theta*\theta)}{(D_r*\theta^4*r^3+D_\theta*\theta^2*r+2*D_1*r^3*\theta^2+4*D_{r\theta}*r^3*\theta^2-2*D_1*r-2*D_\theta*r-4*D_{r\theta}*r+r^3)}*A*\cos(r*\theta)-\frac{(2*D_r*\theta^3*r^2+6*D_1*r^2*\theta+12*D_{r\theta}*r^2*\theta-D_\theta*\theta)}{(D_r*\theta^4*r^3+D_\theta*\theta^2*r+2*D_1*r^3*\theta^2+4*D_{r\theta}*r^3*\theta^2-2*D_1*r-2*D_\theta*r-4*D_{r\theta}*r+r^3)}*B*\sin(r*\theta)+\frac{q*r^4}{D_\theta} \quad (8)$$

It can be applied the boundary conditions on eq. (8) to obtain the constants (A and B):

$$\text{At} r = r_1 = 2.5 \text{ cm}, \theta = \theta_1, w(r,\theta) = 0$$

$$\text{At } r = r_1 = 2.5 \text{ cm}, \theta = \theta_2, w(r,\theta) = 0$$

Where: θ_1 and $\theta_2$vary along each flank and nose profile as shown in Fig.(2).

Then;

$$A = \frac{C_1*C_3*\sec(r_1*\theta_2)*\cos(r_1*\theta_1)*\tan(r_1*\theta_2)-C_2*C_3*\tan(r_1*\theta_2)}{C_1*C_2*(\tan(r_1*\theta_2)*\cos(r_1*\theta_1)-\sin(r_1*\theta_1))}-\frac{C_3*\sec(r_1*\theta_2)}{C_2}$$

$$B = \frac{C_1*C_3*\sec(r_1*\theta_2)*\cos(r_1*\theta_1)-C_2*C_3}{C_1*C_2*(\tan(r_1*\theta_2)*\cos(r_1*\theta_1)-\sin(r_1*\theta_1))}$$

Where:

$$C_1 = \frac{2*D_r*\theta_1^3*r_1^2+6*D_1*r_1^2*\theta_1+12*D_{r\theta}*r_1^2*\theta_1-D_\theta*\theta_1}{D_r*\theta_1^4*r_1^3+D_\theta*\theta_1^2*r_1+2*D_1*r_1^3*\theta_1^2+4*D_{r\theta}*r_1^3*\theta_1^2-2*D_1*r_1-2*D_\theta*r_1-4*D_{r\theta}*r_1+r_1^3}$$

$$C_2 = \frac{2*D_r*\theta_2^3*r_1^2+6*D_1*r_1^2*\theta_2+12*D_{r\theta}*r_1^2*\theta_2-D_\theta*\theta_2}{D_r*\theta_2^4*r_1^3+D_\theta*\theta_2^2*r_1+2*D_1*r_1^3*\theta_2^2+4*D_{r\theta}*r_1^3*\theta_2^2-2*D_1*r_1-2*D_\theta*r_1-4*D_{r\theta}*r_1+r_1^3}$$

$$C_3 = \frac{q*r_1^4}{D_\theta}$$

$$\therefore w(r,\theta) = \frac{(2*D_r*\theta^3*r^2+6*D_1*r^2*\theta+12*D_{r\theta}*r^2*\theta-D_\theta*\theta)}{(D_r*\theta^4*r^3+D_\theta*\theta^2*r+2*D_1*r^3*\theta^2+4*D_{r\theta}*r^3*\theta^2-2*D_1*r-2*D_\theta*r-4*D_{r\theta}*r+r^3)} * \left[\frac{C_1*C_3*\sec(r_1*\theta_2)*\cos(r_1*\theta_1)*\tan(r_1*\theta_2)-C_2*C_3*\tan(r_1*\theta_2)}{C_1*C_2*(\tan(r_1*\theta_2)*\cos(r_1*\theta_1)-\sin(r_1*\theta_1))} - \frac{C_3*\sec(r_1*\theta_2)}{C_2}\right] * \cos(r*\theta) - \frac{(2*D_r*\theta^3*r^2+6*D_1*r^2*\theta+12*D_{r\theta}*r^2*\theta-D_\theta*\theta)}{(D_r*\theta^4*r^3+D_\theta*\theta^2*r+2*D_1*r^3*\theta^2+4*D_{r\theta}*r^3*\theta^2-2*D_1*r-2*D_\theta*r-4*D_{r\theta}*r+r^3)} * \left[\frac{C_1*C_3*\sec(r_1*\theta_2)*\cos(r_1*\theta_1)-C_2*C_3}{C_1*C_2*(\tan(r_1*\theta_2)*\cos(r_1*\theta_1)-\sin(r_1*\theta_1))}\right] * \sin(r*\theta) + \frac{q*r^4}{D_\theta} \quad (9)$$

It can be assumed that the two points of contact load are as the simply-supported beam subjected to distributed load (P_o) per unit length of point loading using superposition theory as illustrated in Fig.(3), [9]:

$$P_o = 0.6 * \sigma_y$$

$$q = P_o * \frac{2*\pi}{3} * \frac{L^2}{8} * \frac{1}{L_1} * \upsilon_F \quad (10)$$

Where:

L: is the length of simply-supported beam.

L_1:is the difference length between two points of contact.

υ_F: is the fiber volume fraction ($\upsilon_F = 0.3$)

The elliptic equation is, [10]:

$$w(x,y) = \frac{q*(\frac{x^2}{a_1^2}+\frac{y^2}{b_1^2}-1)^2}{(\frac{24*D_r}{a_1^4}+\frac{16*H}{a_1^2*b_1^2}+\frac{24*D_\theta}{b_1^4})} \quad (11)$$

Where: a_1 and $b_1$is the major and minor distance axis of ellipse.

And; $H = D_1 + 2*D_{r\theta}$

And the semi-circle equation is, [10]:

$$w(r,\theta) = \sum_{m_1=1,3,5}^{\infty}\left[\frac{4*q*r^4}{\pi*m_1*(16-m_1^2)*(4-m_1^2)*D_r} + A_{1m_1} * r^{m_1} + A_{3m_1} * r^{m_1+2}\right] * \sin(m_1 * \theta) \qquad (12)$$

Where:

$$A_{1m_1} = \frac{-2*q*(m_1+1)*a_2^{4-m_1}}{\pi*m_1*(16-m_1^2)*(4-m_1^2)*D_r}$$

$$A_{3m_1} = \frac{2*q*(m_1-1)*a_2^{2-m_1}}{\pi*m_1*(16-m_1^2)*(4-m_1^2)*D_r}$$

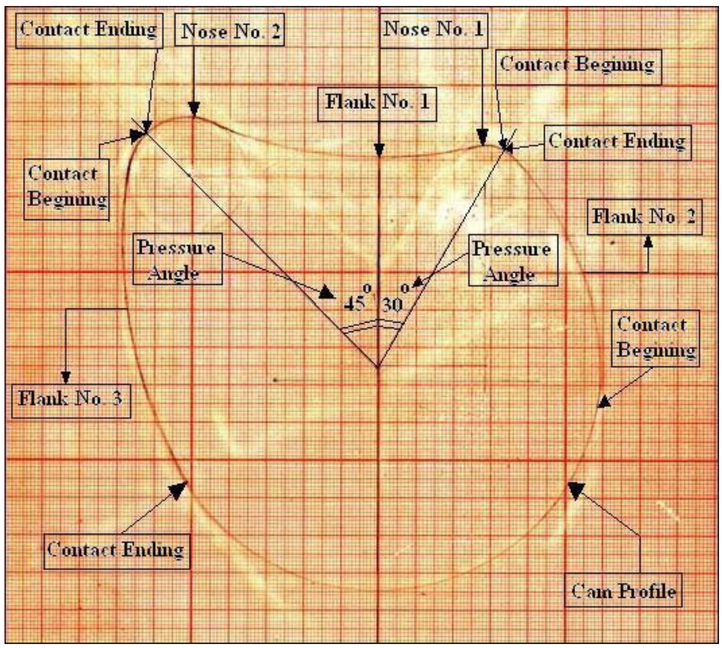

Fig. (2) : Cam Profile Specifications, [11].

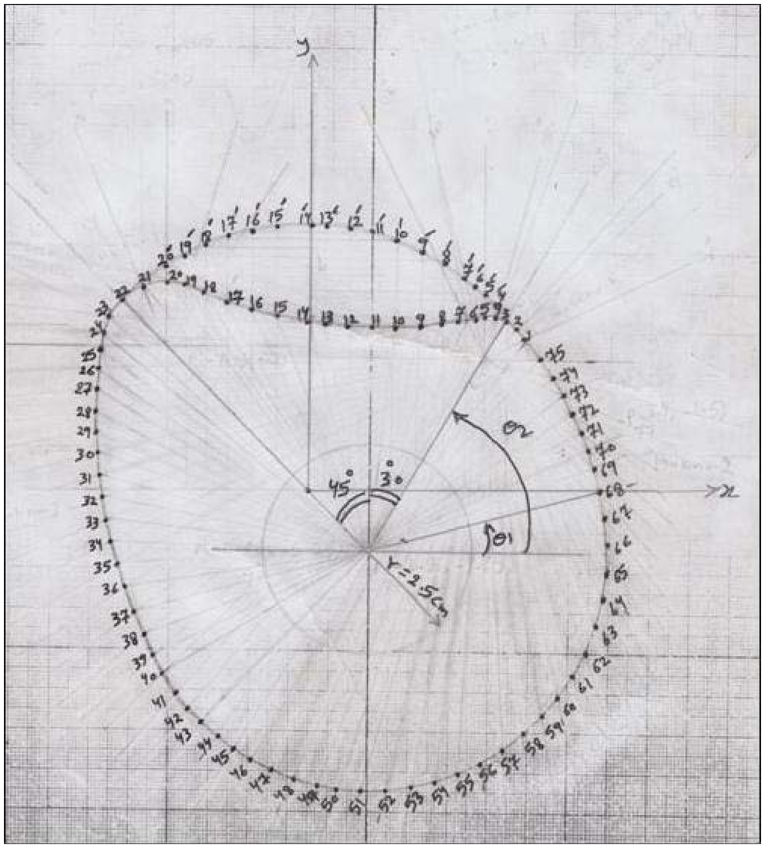

Fig.(3) : The Points of Cam Profile.

IV. Numerical Procedure

For this problem, the (SHELL 99)element is used in this paper for the two-dimensional modeling of orthotropic un-symmetric cam shell structure carried out with ANSYS 12.1 program software and is defined byeight nodes having six degrees of freedom at each node: translations in the nodal x, y, and z directions and rotations about the nodal x, y, and z axes to find the maximum deflection on cam boundaries. The mesh generation of box cam can be indicated in Fig. (4).

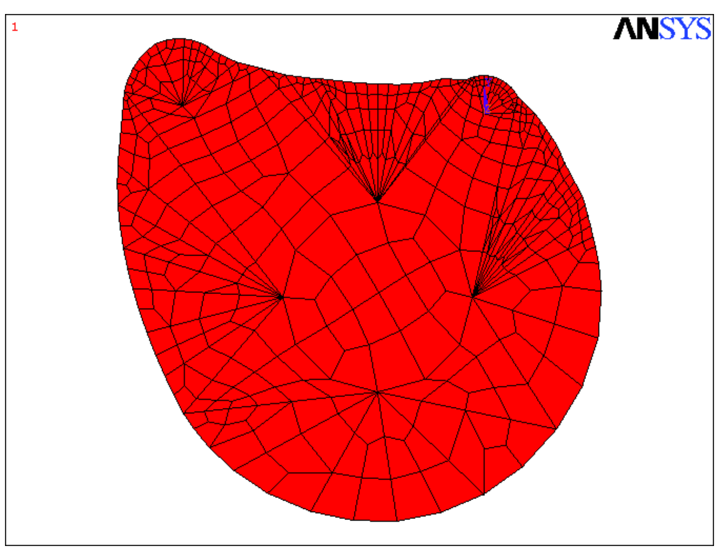

Fig. (4) : The mesh generation of cam un-symmetric cam profile.

V. Results

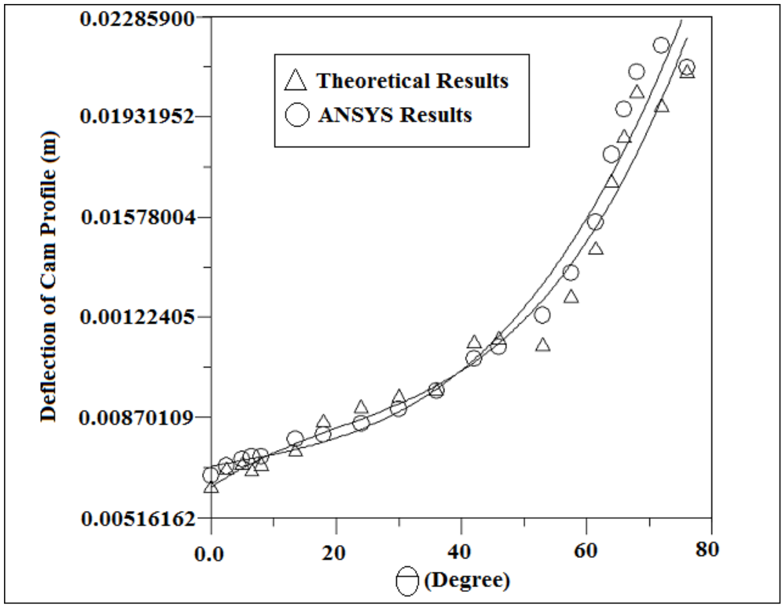

Fig. (5) : Deflection of cam profile against angle of contact for nose no. 1, flank no.1, and nose no. 2.

Fig. (5) shows the deflection of cam profile against angle of contact for nose no. 1, flank no.1, and nose no. 2. The deflection of cam profile increase exponantially with the increasingof the angle of contact for orthotropic cam. The percentage error between theoretical and ANSYS results is closely because the curve degree of orthotropic cam profile is very high.

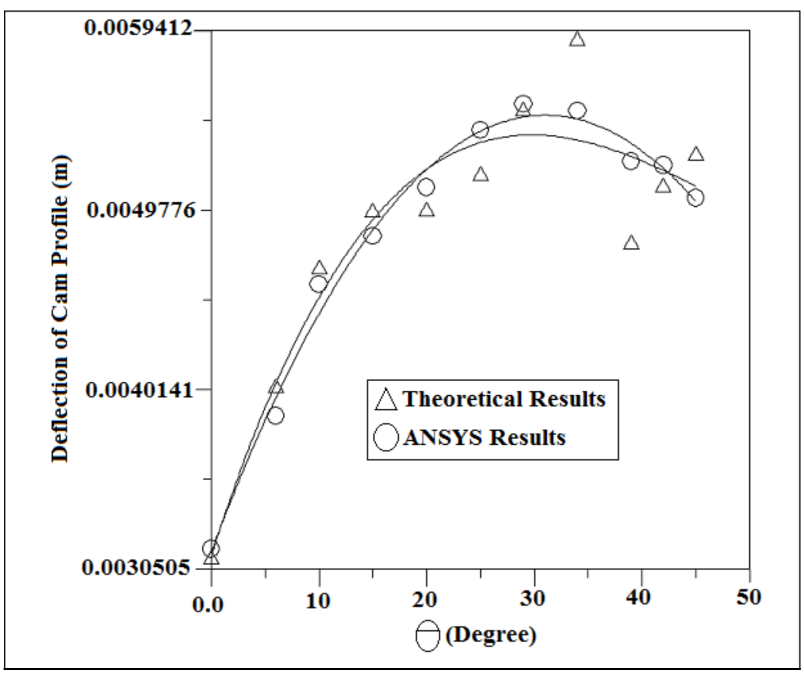

Fig. (6) : Deflection of cam profile against angle of contact for flank no. 2 and nose no. 1.

Fig. (6) shows the deflection of cam profile against angle of contact for flank no. 2 and nose no. 1. The deflection of cam profile vary transiently with the angle of contact for flank no. 2 and nose no. 1 for orthotropic cam. The percentage error between theoretical and ANSYS results is lower than in Fig. (5) because the difference length value between two points of contact (L_1) is accurate.

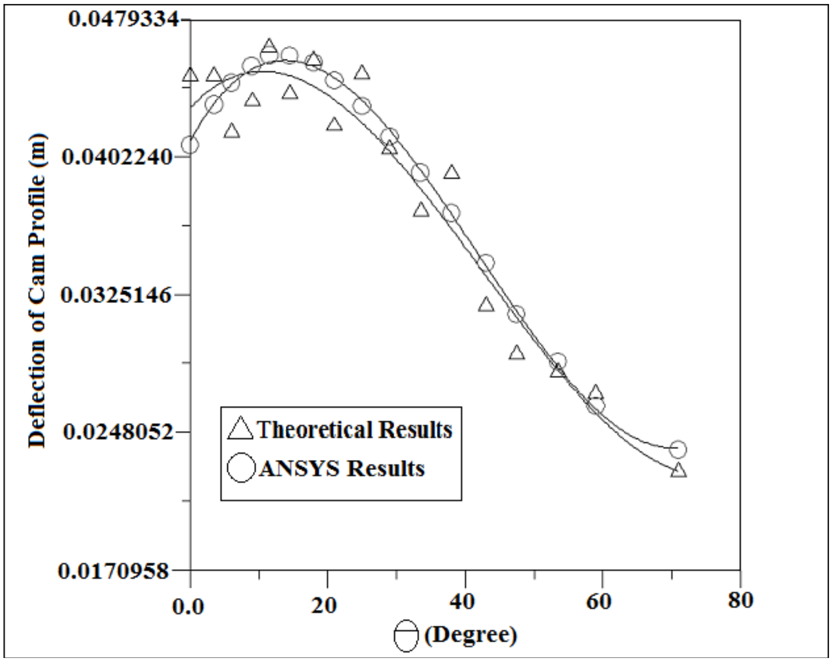

Fig. (7) : Deflection of cam profile against angle of contact for nose no. 2 and flank no. 3.

Fig. (7) shows the deflection of cam profile against angle of contact for nose no. 2 and flank no. 3.The value of deflection decreased sinusoid ally with the increasing of the angle of contact because the contact loading in some locations is small or nearly constant.

Table (1) : Theoretical and ANSYS results for deflection vary with point's numberofnose no. 1, flank no.1, and nose no. 2.

Points Number	Theoretical Results	ANSYS Results	Error (%)
3	0.005161615	0.0056644	8.876%
4	0.0058861	0.006051	2.725%
5	0.00606744	0.0063089	3.827%
6	0.00582013	0.0064287	9.466%
7	0.0060445	0.006436	6.083%
8	0.00661729	0.0071268	7.149%
9	0.00778991	0.0073008	6.278%
10	0.0083432	0.0077435	7.187%
11	0.00878378	0.0083321	5.142%
12	0.00903007	0.0090455	0.17%
13	0.0109305	0.010322	5.566%
14	0.0110767	0.010799	2.507%
15	0.0108222	0.012067	10.31%
16	0.0127715	0.01377	7.251%
17	0.01467905	0.015786	7.012%
18	0.0173589	0.018493	6.132%
19	0.01916212	0.020308	5.642%
20	0.0209437	0.021801	3.932%
21	0.0203995	0.022859	10.76%
22	0.0217526	0.021979	1.03%

Table (1) shows the theoretical and ANSYS results for deflection vary with point's number of nose no. 1, flank no.1, and nose no. 2. The deflection of cam boundary profile increased exponentially with the increasing of point's number on orthotropic cam boundaries because increasing the angle of contact at these points from the point of beginning at nose no.1 to the point of ending at nose no. 2.

Table (2) : Theoretical and ANSYS results for deflection vary with point's number of flank no. 2 and nose no. 1.

Points Number	Theoretical Results	ANSYS Results	Error (%)
68	0.0030505	0.0031101	1.916%
69	0.004008805	0.0038517	3.918%
70	0.00466814	0.0045842	1.798%
71	0.004986	0.0048537	2.653%
72	0.0049904	0.0051238	2.603%
73	0.00519162	0.0054449	4.651%
74	0.0055525	0.0055893	0.658%
75	0.00594125	0.005553	6.691%
1	0.00480574	0.0052705	8.818%
2	0.005125194	0.0052481	2.342%
3	0.005301403	0.0050653	4.453%

Table (2) shows the theoretical and ANSYS results for deflection vary with point's number of flank no. 2 and nose no. 1. The deflection of cam boundary profile increased sinusoid ally with the increasing of point's numbers on orthotropic cam boundaries and the deflection for nose no. (1) is larger than the deflection of flank no. (1) because the effect of the radius of curvaturesfrom the point of beginning at flank no. 2 to the point of ending at nose no. 1.

Table (3) : Theoretical and ANSYS results for deflection vary with point's number of nose no. 2 and flank no. 3.

Points Number	Theoretical Results	ANSYS Results	Error (%)
22	0.0458897	0.040823	11.041%
23	0.0458858	0.043772	4.606%
24	0.0418067	0.045346	7.805%
25	0.0440422	0.046558	5.403%
26	0.0479334	0.047361	1.194%
27	0.04459053	0.047317	5.762%
28	0.0470031	0.046831	0.3661%
29	0.04224056	0.045533	7.231%
30	0.0460082	0.043685	5.049%
31	0.0405565	0.041455	2.167%
32	0.0360775	0.038849	7.134%
33	0.0387652	0.035871	7.466%
34	0.029147	0.032265	9.663%
35	0.0256657	0.028528	10.033%
36	0.02435666	0.025104	2.977%
37	0.02280797	0.021889	4.029%
39	0.0170958	0.018668	8.421%

Table (3) shows the theoretical and ANSYS results for deflection vary with point's number of nose no. 2 and flank no. 3. The deflection of cam boundary profile decreased transiently with the increasing of point's number on orthotropic cam boundaries because varying the radius of curvature at these points from the point of beginning at nose no. 2 to the point of ending at flank no. 3.

VI. Conclusions

1) The deflection of orthotropic cam is larger than the deflection in isotropic cam because the modulus of elasticity and Poisson's ratio for orthotropic cam is small for the same contact loading.
2) The maximum deflection occurs at nose no. (2) because the radius of curvature is small.
3) The deflection on noses is larger thanthe deflection of flanks because the effect of the radius of curvatures.

References Références Referencias

1. Harald Müller, MWP Mahle, J. Wizemann, Pleuco GmbH, and Andreas Kaiser, "Composite Camshaft- Avoid Lobe Grinding Using PM Lobes", Journal of SAE, No. 970001, 24-2-2007.
2. kong Fan-feng1, CHU Chao-meil, WANG Bo2, and LI Zhao-jian1, "Design and Study of New Composite Function Cam Profile", Chinese Journal,12-1-2011.
3. LeventCenkKumruoǧlu, " Mechanical and Microstructure Properties of Chilled Cast Iron Camshaft: Experimental and Computer Aided Evaluation ", Journal of Materials and Design, No. 33, pp. 927-938, 2009.
4. Pei QuanGuq, ShouRen Wang, and Huan Yong Cui," Microstructure and Properties of Ti Al N/Al N Composite Film Deposited on Cam's Profile by Ion Beam Sputtering Technique", Journal of Key

Engineering Materials, Vol. 443, pp. 465-468, June 2010.

5. ZHANG Chi, LI Yue-ying, YANG Shen-hua, and LIU Yong-bing, “The Study of Cam Materials and Assembling Technology of Composite Hollow Camshafts", Chinese Journal (Material Science and Technology), 3-1-2005.
6. Eric M. Chappelear, and William J.Hacker, “Composite Shifter Cam for A Motorcycle Transmission", Track new patents and Technologies, 2006.
7. R. Purohit, and R. Sagar, "Fabrication of A Cam using Metal Matrix Composites", Journal of Advanced Manufacturing Technology , No. 9, Vol. 17, pp. 644-648, 2001.
8. James F. Wilson, “Impact-Induced Fatigue of Foamed Polymers ", Journal of Impact Engineering, No. 34, pp. 1370-1381, 2007.
9. E. J. Hearn, "Mechanics of Materials", Book of second edition, Volume 2, 1985.
10. Eduard Ventsel, and Theodor Krauthammer, "Thin Plates and Shells", Book of Theory, Analysis and Application, 2001.
11. Yu and H P Lee, "Size Optimization of Cam Mechanisms with Translating Roller Followers", Journal of Mechanical Engineering Science, Vol. 212, No. C5, 1998.

This page is intentionally left blank